Effect of machining conditions on the trimming damage in composite laminates induced by out-of-plane shearing

Yashiro, Shigeki
Department of Aeronautics and Astronautics, Kyushu University

Ono, Ryuji
Department of Mechanical Engineering, Shizuoka University

Ogi, Keiji
Graduate School of Science and Engineering, Ehime University

出版情報：Journal of Materials Processing Technology. 271, pp.463-475, 2019-09-01. Elsevier
バージョン：
権利関係：

Title: Effect of machining conditions on the trimming damage in composite laminates induced by out-of-plane shearing

Authors: Shigeki Yashiro, Ryuji Ono, Keiji Ogi

PII: S0924-0136(19)30147-5
DOI: https://doi.org/10.1016/j.jmatprotec.2019.04.025
Reference: PROTEC 16199

To appear in: *Journal of Materials Processing Technology*

Received date: 4 October 2018
Revised date: 11 March 2019
Accepted date: 10 April 2019

Please cite this article as: Yashiro S, Ono R, Ogi K, Effect of machining conditions on the trimming damage in composite laminates induced by out-of-plane shearing, *Journal of Materials Processing Tech.* (2019), https://doi.org/10.1016/j.jmatprotec.2019.04.025

Effect of machining conditions on the trimming damage in composite laminates induced by out-of-plane shearing

Shigeki Yashiro [1,*], Ryuji Ono [2], Keiji Ogi [3]

[1] Department of Aeronautics and Astronautics, Kyushu University

744 Motooka, Nishi-ku, Fukuoka 819-0395, Japan

[2] Department of Mechanical Engineering, Shizuoka University

3-5-1 Johoku, Naka-ku, Hamamatsu 432-8561, Japan

[3] Graduate School of Science and Engineering, Ehime University

3 Bunkyo-cho, Matsuyama, Ehime 790-8577, Japan

* Corresponding author: yashiro@aero.kyushu-u.ac.jp (S. Yashiro)

Abstract

Fast machining is essential for mass production of composite structures, and out-of-plane shearing, also known as die cutting, is appropriate for trimming. Nevertheless, little is known about shearing of polymer-matrix composites. This study was done to investigate the

damaging impact of shearing conditions on carbon fiber reinforced plastic (CFRP) laminates. The clearance and temperature affected the damage progress, while the cutting speed in the tested range had negligible effect. In cross-ply laminates, delamination and matrix cracks first appeared in a narrow shearing zone, and with further loading longitudinal plies broke at the dies' edges. Although delamination occurred only in a narrow shear-stress concentrated zone in the case of a small clearance, it was significant for a large clearance, owing to the local bending deformation. A temperature slightly lower than the glass transition temperature narrowed the delamination area, owing to the increase in the interlaminar fracture toughness as well as insignificant strength degradation of the matrix.

Keywords: Carbon fiber reinforced plastics (CFRPs); Trimming; Die cutting; Delamination; Matrix cracks

1. Introduction

Recently, significant effort has been made to use carbon fiber reinforced plastics (CFRPs) in automobile structures, for weight reduction and improvement of fuel efficiency. However, CFRP products are generally expensive owing to their high material and production costs, and are seldom used in general-purpose equipment. Facility occupation time is an important factor that affects productivity; therefore, appropriate machining methods are required for mass

production of composite structures. Finish machining is necessary for composite structures, even if components are molded in near-net shapes.

Milling (Gordon and Hillery, 2003; Che et al., 2014; Soussia et al., 2014) and abrasive waterjets (Wnag, 1999; Kalla et al., 2012; Alberdi et al., 2013) have been widely used for trimming. Milling induces extensive wear of tools and put high thermo-mechanical loading to CFRPs by heating up in the working area. Machining-incurred damage as well as rapid wear of cutting tools have been investigated for standard machining such as turning, drilling and milling (Teti, 2002; Davim and Reis, 2005; Hintze et al., 2011; Sheikh-Ahmad et al., 2012). Temperature elevation was measured during milling process of CFRPs (Yashiro et al., 2013). Abrasive waterjet also causes delamination, and its mechanism has been investigated experimentally and analytically (MM et al., 2018; Shanmugam et al., 2008; Schwartzentruber et al., 2018). Its optimal feed rate is generally low, and moisture absorption is an undesirable issue for CFRPs. In recent years, laser cutting of CFRPs has been studied (Dubey and Yadava, 2008). Great difference in material properties between fibers and matrix causes heat-affected zone during absorption of high thermal energy (Li et al, 2010), and its minimization is a major topic in laser cutting of CFRPs (Fürst et al., 2017; Leone and Genna, 2018; Li et al., 2018). Machining quality in polymer-matrix composites by the above three techniques has been compared (Shanmugam et al., 2002; Hejjaji et al., 2016). However, these techniques take a long time to cut long edges, because these methods require to follow the machining path to

obtain prescribed shapes, and because the kerf quality is negatively correlated with the machining speed. This inherent characteristic results in low productivity. From the viewpoint of the machining speed, out-of-plane shearing (also known as die cutting) can be used for trimming.

Out-of-plane shearing has been used frequently in metal processing for mass production. By contrast, there are only a few studies on the out-of-plane shearing of composite materials, probably because severe delamination is usually assumed. However, our previous studies (Yashiro et al., 2014; Nakamura et al., 2015; Yashiro and Ogi, DOI: 10.1177/0021998318801454) suggested that thermoset CFRP laminates can be cut by out-of-plane shearing without inducing extensive delamination growth. Watzke et al. (2014) performed cryogenic shearing of woven composites, aiming at the embrittlement of the underlying matrix. They obtained a sharp cut surface under cryogenic conditions, while the burr remained at room temperature. Tatsuno et al. (2018) cut textile carbon fiber reinforced thermoplastic (CFRTP) laminates and observed a shaggy fracture pattern at the center of the samples' thickness dimension. Their observation was limited to the ply-scale; the detailed mechanism of damage accumulation by out-of-plane shearing remains unclear.

Determining optimal machining conditions is important for composite structures, because machining-incurred damage always degrades the mechanical properties of composites (Persson et al., 1997; Saleem et al., 2013; Haddad et al., 2014; Li et al., 2018; Herzog et al.,

2008). With respect to the out-of-plane shearing of composites, the process of damage accumulation was observed in a simple cross-ply laminate (Yashiro et al., 2014; Yashiro and Ogi, DOI: 10.1177/0021998318801454), but none of the previous studies have systematically revealed the influence of shearing conditions on the accumulation of damage. The cutting speed, the clearance between the upper and lower dies, the temperature of the workpiece, and the shape of the cutting die typically affect the process of damage accumulation leading to shear cutting. Clear understanding of the effect of these parameters is essential for optimizing the shearing process.

Owing to the lack of experimental observations and analytical suggestions, we studied the feasibility of out-of-shearing of composite laminate plates with fundamental stacking sequences, to understand the mechanism of damage accumulation and to explore appropriate machining conditions. In particular, this study was done to systematically investigate the influence of the clearance, cutting speed, and temperature on the damage accumulation in composite laminates. The present study demonstrates the use of the simplest shape of the cutting die; the effect of the die shape on the final quality was investigated by Nakamura et al. (2015). Determining the conditions that minimize the machining-incurred damage in CFRP laminates is a step forward toward developing processing methods that incur no shearing damage in CFRTPs, which are promising materials for automotive applications.

This article is organized as follows. First, the material used and the experimental procedure

are described in Section 2. In Section 3, the damage accumulation process in CFRP laminates is presented in terms of the cutting speed (Section 3.1), clearance between the upper and lower dies (Section 3.2), and temperature (Section 3.3). Section 4 presents a mathematical model to predict the maximal shear stress during out-of-plane shearing, and suggests appropriate machining conditions. Finally, Section 5 summarizes the mechanism of the evolution of the damage incurred by out-of-plane shearing.

2. Experiment

Carbon fiber reinforced epoxy prepreg sheets (T700S/#2592, Toray Industries) were used in the present study. Four fundamental stacking sequences were considered; namely, unidirectional laminations $[0_8]$ (UD0) and $[90_8]$ (UD90), simple cross-ply lamination $[0_2/90_2]_S$ (CP1), and cross-ply lamination with many ply interfaces $[0/90]_{2S}$ (CP2). The laminates were cured at 130°C, at 0.2 MPa, for 2 hours, using a hot-press machine with a vacuum chamber. Coupon specimens were cut out from the laminates using a diamond saw, and each coupon specimen was 40 mm long, 10 mm wide, and 1.1 mm thick. Figure 1 depicts the morphology of a CP1 specimen, where 0° is the longitudinal direction of a coupon. This study focuses on the major types of damage affecting integrity of the composite material, namely transverse cracks, interlaminar delamination and fiber breaks. The glass transition temperature T_g of the fabricated CFRP laminates was measured using a thermal analysis instrument (DTA60-A,

Shimadzu), and T_g was determined as 92°C.

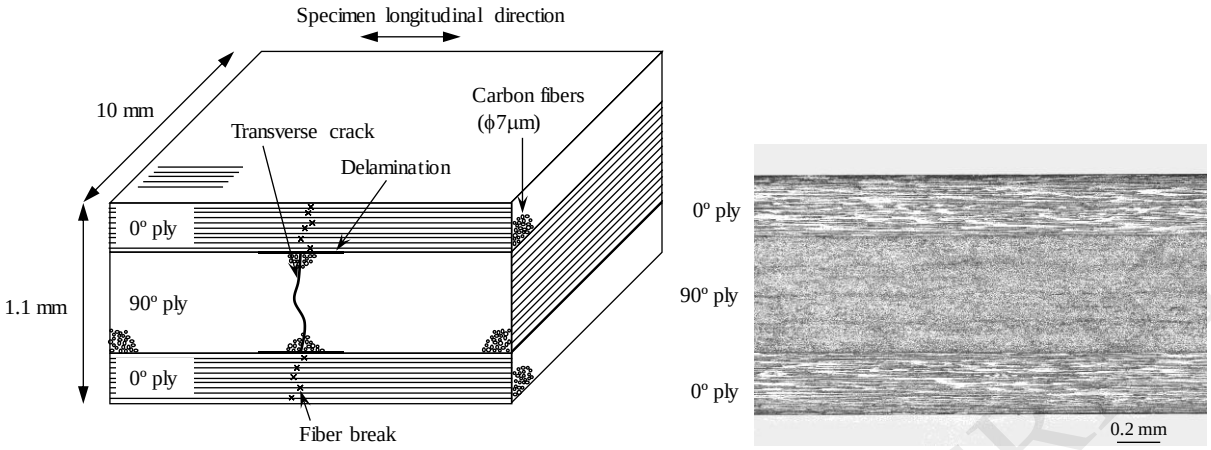

(a) Schematic (b) Micrograph of the specimen edge

Figure 1 Morphology of a composite laminate. The CP1 lamination is depicted as an example.

Figure 2 shows the schematic of the shearing jig. The upper jig moved along a vertical guide pole, to prevent inclination of the upper die. This study used flat blades as a fundamental cutting die; more specifically, the knife angle and the shearing angle were zero, for both the upper and lower dies. The dies were made of flame-hardened steel with good hardness, machinability, toughness, and durability. A part of the specimen (30 mm of its length) was fixed on the lower jig using a stopper plate, and the remaining 10-mm-long part was cut down. The stopper plate was screwed in place using two bolts with springs between them. The jig was placed on a universal testing machine (AG-50kNXplus, Shimadzu), and the upper jig was slid down to cut a coupon specimen. The load and the crosshead displacement were measured during the test. The edges of the cut specimens were observed using an optical microscope, and soft X-ray radiography (M-100, Softex) was used for determining delamination. Furthermore, some additional specimens were removed from the jig in the

middle of shearing, to observe damage accumulation.

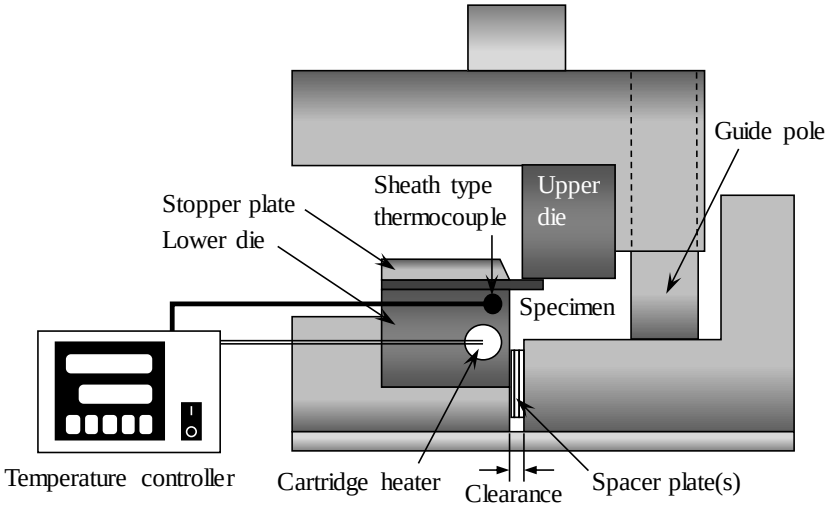

Figure 2 Schematic of the out-of-plane shearing jig.

The clearance (i.e., the horizontal distance between the upper and lower dies), the specimens' temperature, and the cutting speed were all considered as machining conditions. The clearance (0.01 mm to 0.50 mm) was adjusted by inserting thin spacer plates between the lower die and the jig body. The temperature of the specimens was controlled using a cartridge heater inserted into the lower die. The specimen temperature was determined using a pre-measured calibration curve between the specimen temperature and a designated value.

3. Results and discussion

3.1 Cutting speed

First, the UD0 specimens were tested for some cutting speeds, under three clearance conditions. In this study, the crosshead indentation speed was varied (1, 100, and 1000 mm/min), but it should be noted that the actual cutting speed is not identical to the indentation

speed. Figure 3 shows typical shear stress-displacement curves; the shear stress is the load divided by the cross-sectional area. The shear stress initially increased with an increase in displacement, independent of the clearance. Near the maximal stress, the displacement increased without a significant change in the stress. This suggests that the longitudinal plies were cut progressively under a nearly constant shear stress. The shear stress decreased steeply as the displacement increased further. The specimens were almost cut at the stress drop. The indentation speed did not alter the overall trend of the shear stress-displacement diagram, such as the initial slope and the maximal stress.

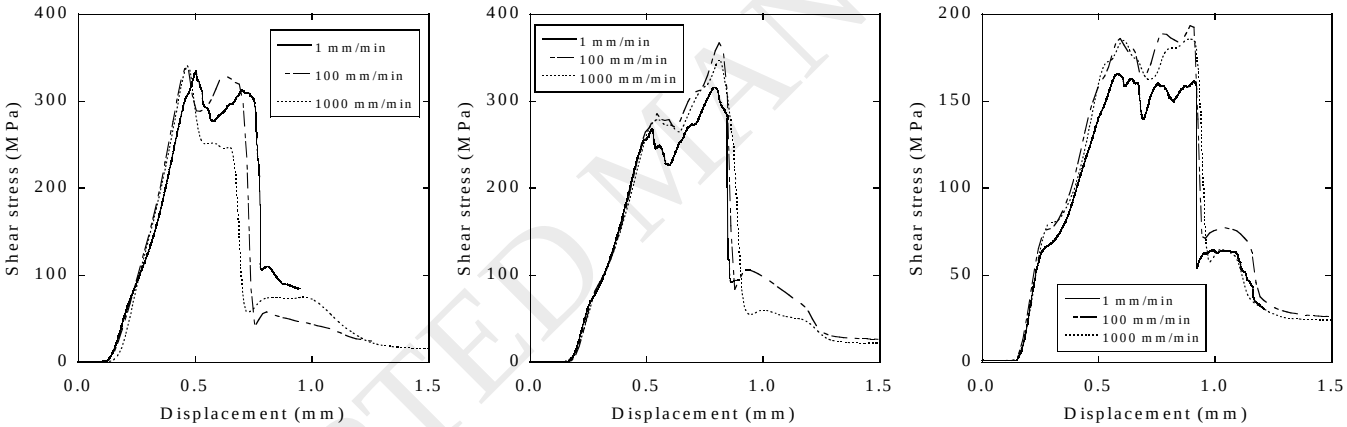

(a) 0.05 mm clearance (b) 0.2 mm clearance (c) 0.5 mm clearance

Figure 3 Shear stress-displacement curves for the UD0 specimens, for different indentation speeds.

The failure displacement led to the appearance of permanent deformation in the shearing zone, with an inclined cut surface (called 'shear drops'), as shown in Fig. 4a, and the angle between the bottom surface and the major cut surface is shown in Fig. 4b. As the indentation speed increased, the cut angle slightly approached the right angle.

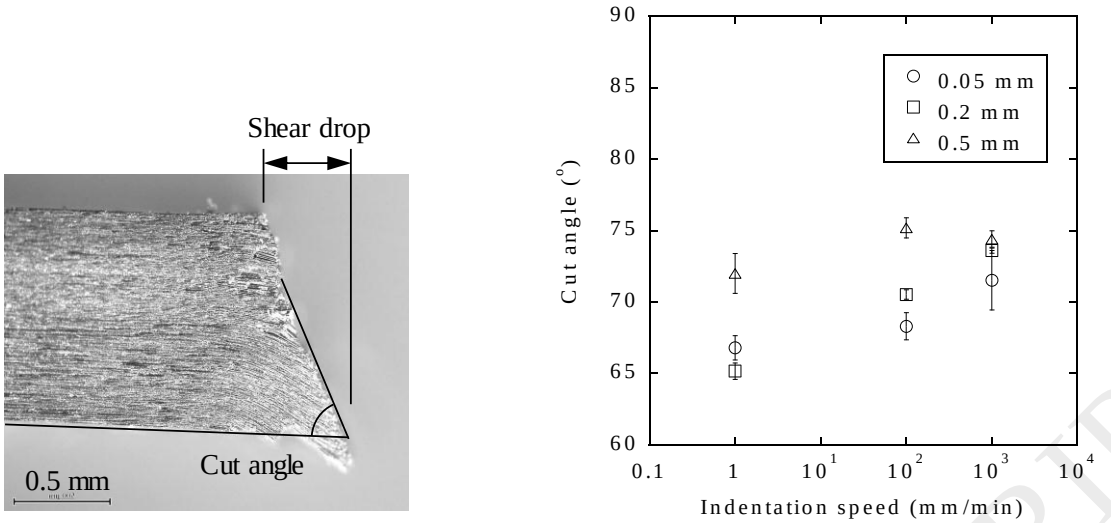

(a) Appearance of the specimen (b) Relationship between the cut angle and the indentation speed

Figure 4 Inclination of the cut surface against the bottom plane. Error bars in panel (b) indicate the standard deviation.

The above results demonstrate that the effect of the indentation speed was negligible within the tested range of speed values. Therefore, hereafter the indentation speed was fixed at 1 mm/min for in-situ observations. However, the practical cutting speed (~1 m/s for metals) is much higher than the maximal speed in this study, which necessitates additional research. It should be noted that shearing takes a short time to cut a long edge even at a low indentation speed compared with milling and abrasive waterjet.

3.2 Clearance

The specimens were cut under four clearance conditions (0.05, 0.1, 0.2, and 0.5 mm) to clarify the effect of the clearance on the accumulation of damage. The specimens used were the unidirectional laminates UD0 and UD90, and the simple cross-ply laminate CP1. All of

the tests were conducted at room temperature.

Figure 5 shows typical shear stress-displacement curves for the UD0 specimens. The maximal stress decreased and the displacement at the steep stress drop increased with an increase in clearance, although all of the curves had similar shapes. When the load was removed after a slight change in the slope at the initial stage of the loading, the specimens bent locally between the upper and lower dies, suggesting a plastic deformation and a microscopic damage of the matrix. Figure 6 shows the micrographs of the specimens' edge, just before the drop of the applied stress. Fibers broke near the edge of the dies at the maximal stress. In the case of a large clearance (0.5 mm), lateral cracks (arrow A) appeared in the center of the specimen thickness dimension, and additional fiber breaks (arrow B) were generated apart from the lower die. The displacement increased at a high stress owing to progressive fiber breaks. Most fibers were cut by further indentation of the upper die, and the stress decreased steeply. The shear stress then decreased gradually owing to the load bearing of remaining fibers, such as burrs on the lateral sides.

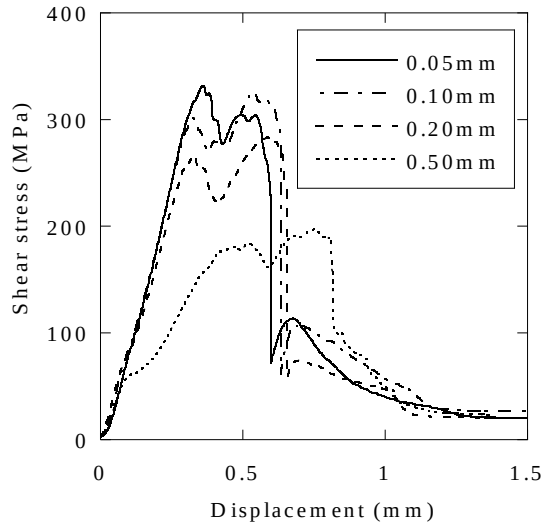

Figure 5 Shear stress-displacement curves for the UD0 specimens, for four clearances.

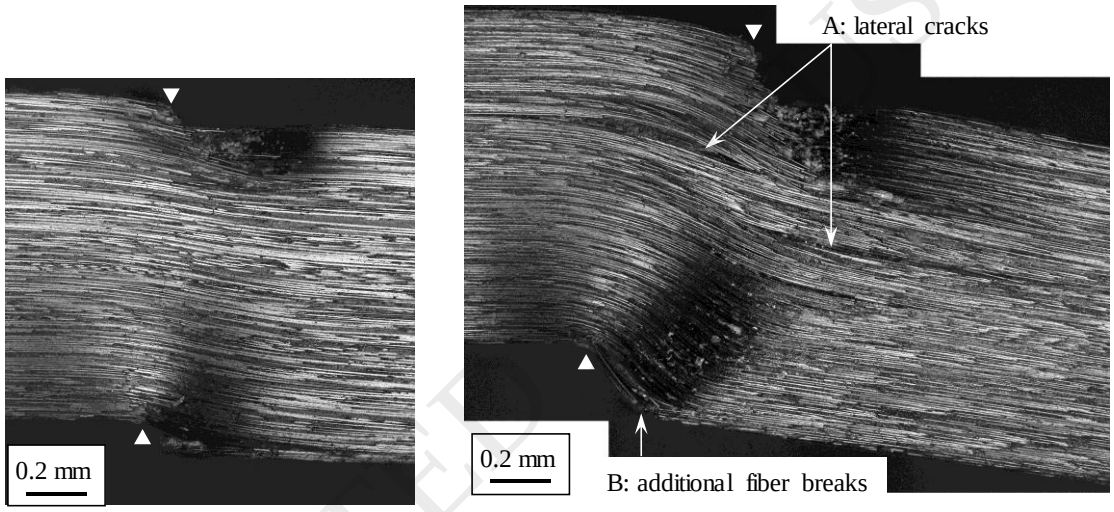

(a) 0.05 mm clearance (b) 0.5 mm clearance

Figure 6 Edge observations for the UD0 specimen after the onset of fiber breaks. Triangles indicate the tips of the upper and lower dies.

Figure 7 shows the shear stress-displacement curves for the UD90 specimens. The shear stress increased monotonically with an increase in displacement in the case of the 0.05-mm-wide clearance. There was no macroscopic plastic deformation before the maximal shear stress. A crack was generated and extended from the tip of the upper die to the tip of the lower die (Fig. 8a), which caused a steep drop in the stress. In the case of the 0.5-mm-wide

clearance (Fig. 8b), a crack (arrow A) was first generated in the fixed part owing to the local bending deformation, which caused a temporal drop in the stress. The fixed part could move upward slightly since the specimen was clamped by hard springs, intending a marginal reduction of the maximal shear stress by the local bending deformation. The first crack did not penetrate the thickness of the specimen, and the shear stress increased again with further indentation. The second major crack (arrow B) then occurred at the same stress as for the small clearance case, and the specimen broke completely.

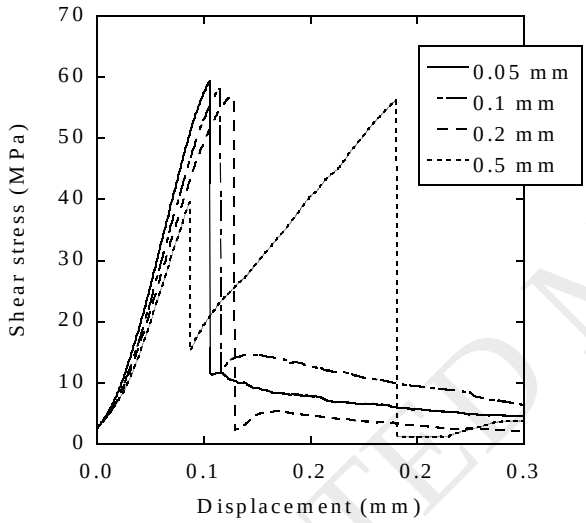

Figure 7 Shear stress-displacement curves for the UD90 specimens, for four clearances. In the case of 0.1 mm and 0.2 mm clearances, two-peak curves were also obtained for some specimens.

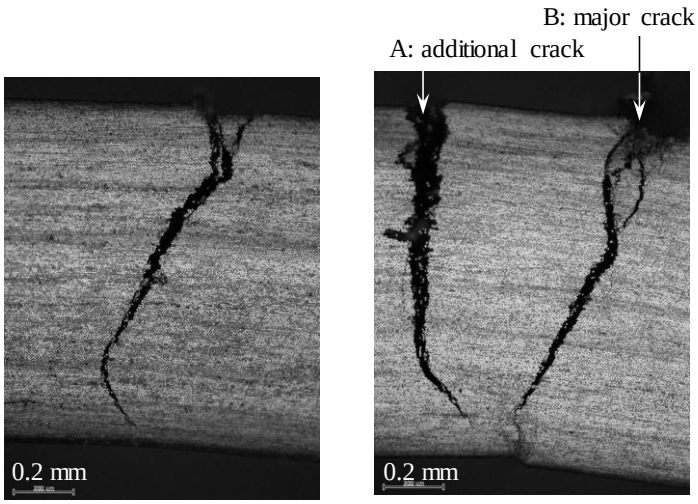

(a) 0.05 mm clearance (b) 0.5 mm clearance

Figure 8 Edge observations for the UD90 specimens immediately prior to the complete cut-off.

The characteristics of the UD0 and UD90 were determined from the results for the CP1 specimens. Figure 9 shows the shear stress-displacement curves for the CP1 specimens, and Fig. 10 shows the micrographs of the specimens' edge at the middle stages of testing. The shear stress increased monotonically, and the slope changed at the displacement near the failure displacement of the UD90 specimens. This slight change in the slope was caused by the small delamination at the 0°/90° interface and the onset of transverse cracks. The stress increased with an increase in displacement, and the damage state remained almost unchanged until reaching the maximal stress (Fig. 10(ii)). The stress then dropped abruptly owing to fiber breaks in the upper 0° ply (Fig. 10(iii)). The upper 0° ply was cut obliquely to the top surface to form the shear drop, and the major transverse crack that connected the upper and lower dies appeared in the 90° ply (Fig. 10(iv)). In the case of the large clearance, additional cracks were generated in the shearing zone (Fig. 10b(iv)). Further, the upper and lower 0°/90° interfaces

were delaminated.

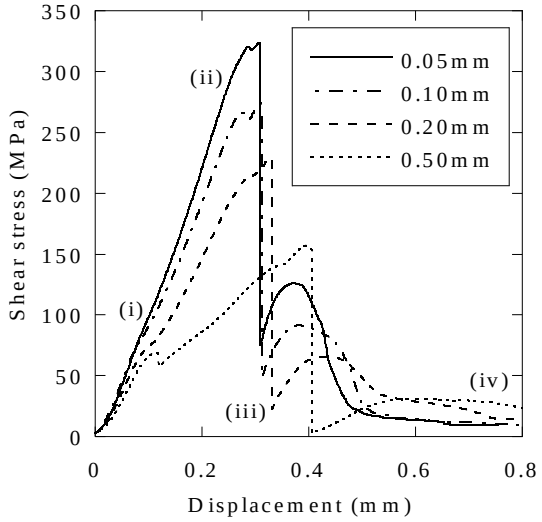

Figure 9 Shear stress-displacement curves for the CP1 specimens, for four clearances.

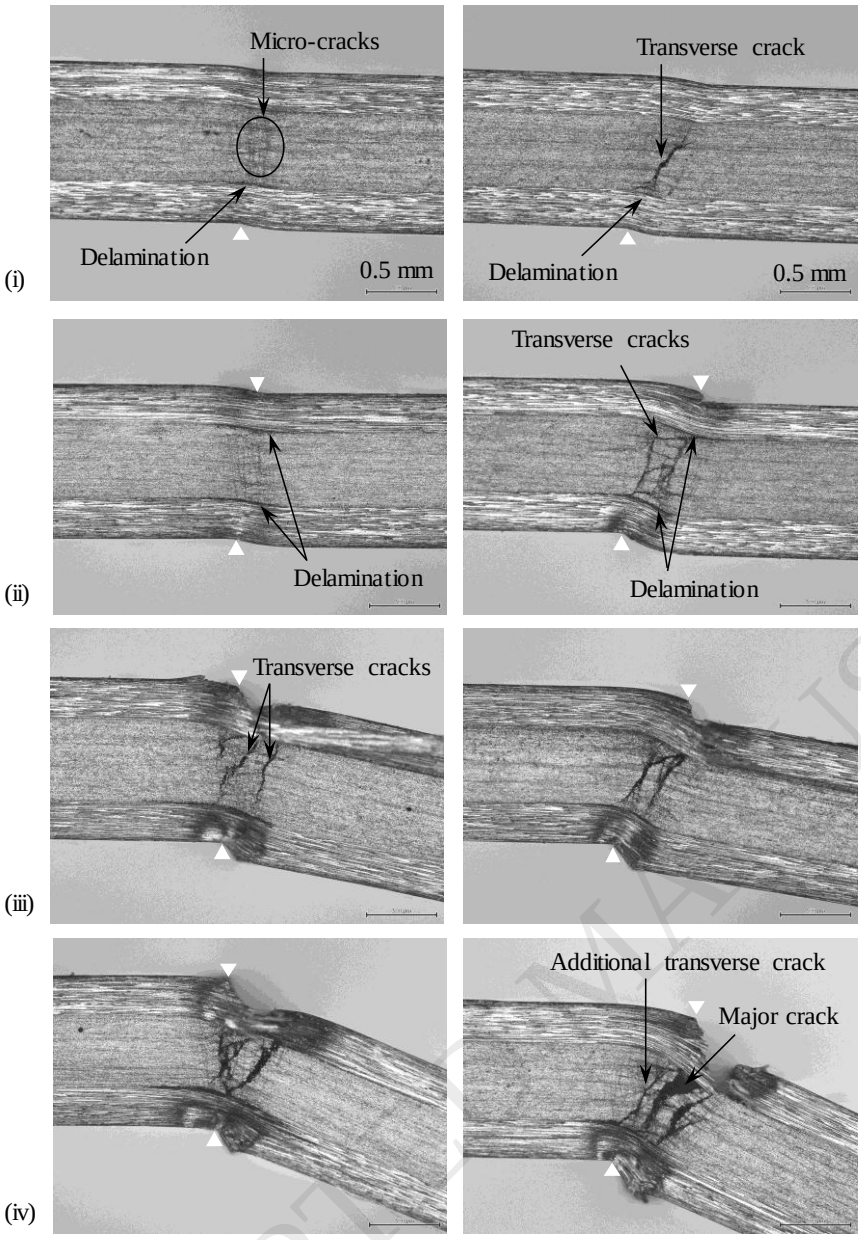

(a) 0.05 mm clearance (b) 0.5 mm clearance

Figure 10 Accumulation of damage in the CP1 specimens tested at room temperature: (i) after slight slope change, (ii) before reaching the maximal stress, (iii) after the steep drop in the stress, and (iv) after further indentation for complete cut-off. The stress levels (i)-(iv) are indicated in Fig. 9.

A larger clearance generated a larger local bending deformation between the upper and lower dies that induced additional cracks in the 90° ply and led to the formation of a larger delamination area. Figures 11a and 11b show the residual damage in the CP1 specimens after

complete cut-off. Delamination was observed in the fixed side coupon after complete cut-off, and in the case of the large clearance (Fig. 11b) a transverse crack also remained in the 90° ply. Delamination in the fixed side coupon was observed using soft X-ray radiography (Fig. 11c). The delamination length was almost constant along the specimens' width dimension, and the projected delamination area decreased almost linearly with a decrease in the clearance.

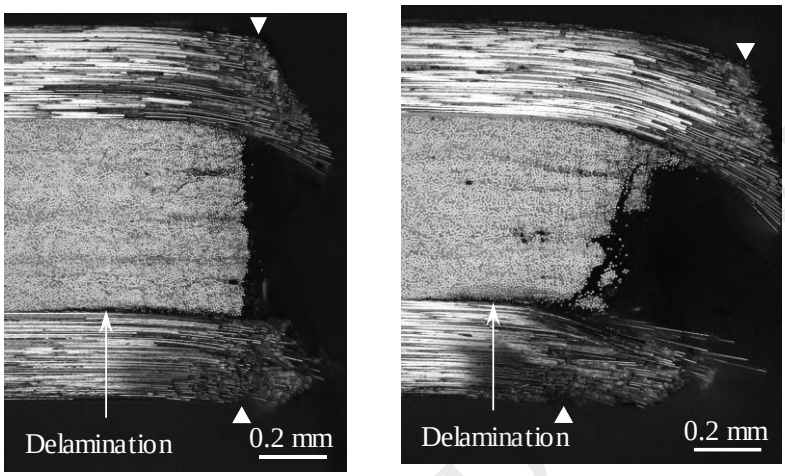

(a) 0.05 mm clearance (b) 0.5 mm clearance

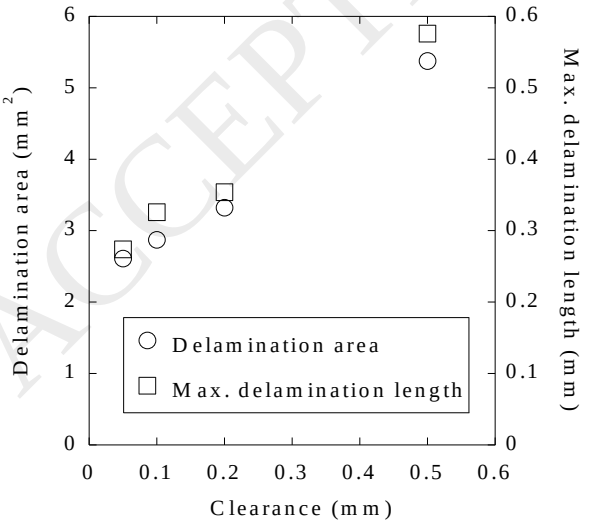

(c) Delamination area versus clearance

Figure 11 Cut quality of the CP1 specimens, vs. the clearance.

3.3 Temperature

Out-of-plane shearing was conducted at high temperatures (70°C, 90°C, and 110°C) to investigate the influence of temperature on the machining-induced damage, while the glass transition temperature T_g of the tested material was 92°C. Similar to the results obtained at room temperature, a larger clearance induced a more severe machining damage in all of the stacking sequences. Therefore, in what follows we describe the results obtained for the 0.05-mm-wide clearance.

Figure 12 shows the results for the UD0 specimens tested at different temperatures. The shear stress-displacement curves for the UD0 specimens (Fig. 12a) reveal that the maximal stress does not change much with temperature, because the strength properties of carbon fibers were not affected by the considered temperatures. The fixed side coupon tested at a temperature lower than T_g (Fig. 12b) exhibited similar appearance to the coupon tested at room temperature (Yashiro and Ogi, DOI: 10.1177/0021998318801454); there was no obvious damage. At a temperature higher than T_g, a lateral crack (arrow A) was generated at the center of the specimen thickness dimension, and a straight fiber-break line (arrow B) appeared in the fixed side (Fig. 11c), which caused a plateau in the shear stress before reaching the maximal stress. The shear stress decreased gradually after reaching the maximal stress, probably because of the fiber/matrix debonding observed within 1 mm from the cut surface (Fig. 12c).

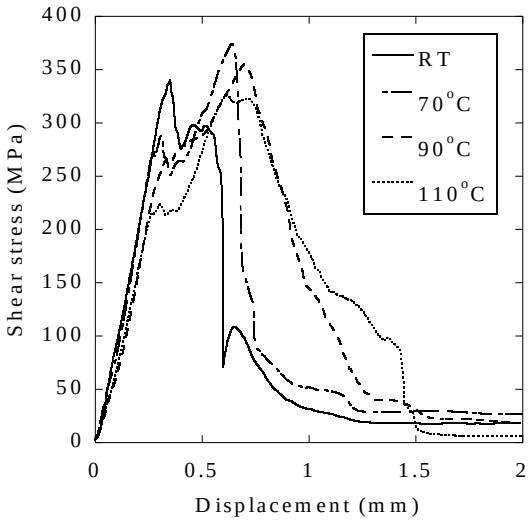

(a) Shear stress-displacement curve

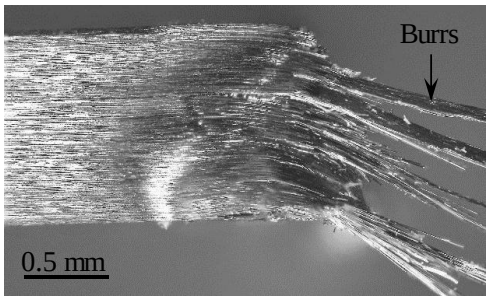

(b) Edge observation (70ºC)

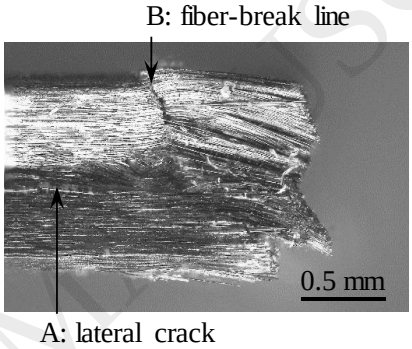

(c) Edge observation (110ºC)

Figure 12 Results for the UD0 specimens, for four temperatures.

Figure 13 shows the results for the UD90 specimens. The maximal stress decreased with an increase in temperature, and the shear stress decreased gradually after reaching the maximal stress at a high temperature (Fig. 13a). An additional crack was generated at the fixed side despite the small clearance (Figs. 13b and 13c). These results suggest softening of the matrix at a high temperature near T_g.

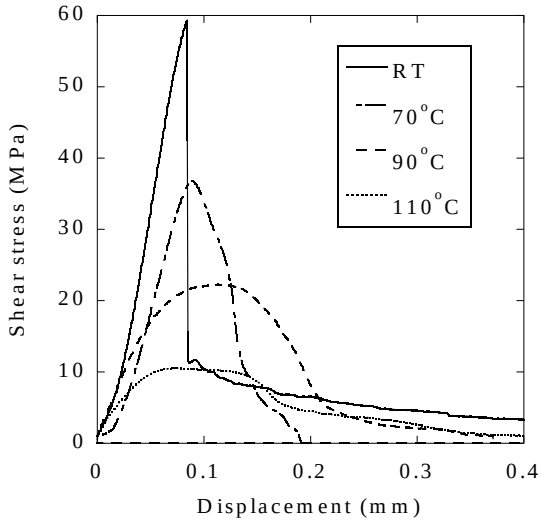

(a) Shear stress-displacement curve

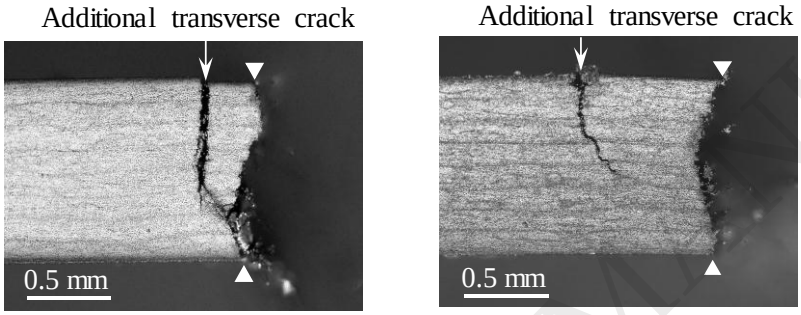

(b) Edge observation (70ºC) (c) Edge observation (110ºC)

Figure 13 Results for the UD90 specimens, for four temperatures.

In the case of multi-directional lamination, temperature dependence of the interlaminar properties, as well as softening of the matrix, affected the damage progress. Figure 14 shows the shear stress-displacement curves for the CP1 laminates, tested at different temperatures. The overall trend was nearly the same, because the cutting process was dominated by the fibers. The edge observations for the CP1 specimens cut at 70°C and 110°C are shown in Fig. 15, which reveals that the damage accumulation process at 70°C is almost the same as that at room temperature (Fig. 10a). Delamination and micro-cracks in the 90° ply occurred in the

narrow shearing zone during the initial stage of the loading. With an increase in displacement, the micro-cracks coalesced into a transverse crack, followed by fiber breaks in the 0° plies. In the specimen that was cut at 110°C, a transverse crack remained on the fixed side, and delamination was much larger than for the specimen that was cut at 70°C.

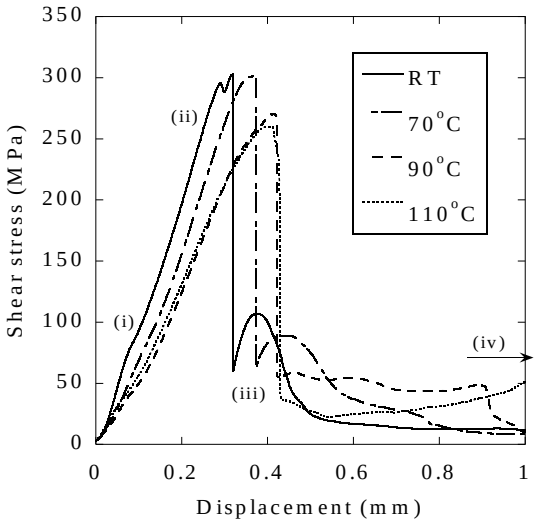

Figure 14 Shear-stress displacement curves for the CP1 specimens, for four temperatures.

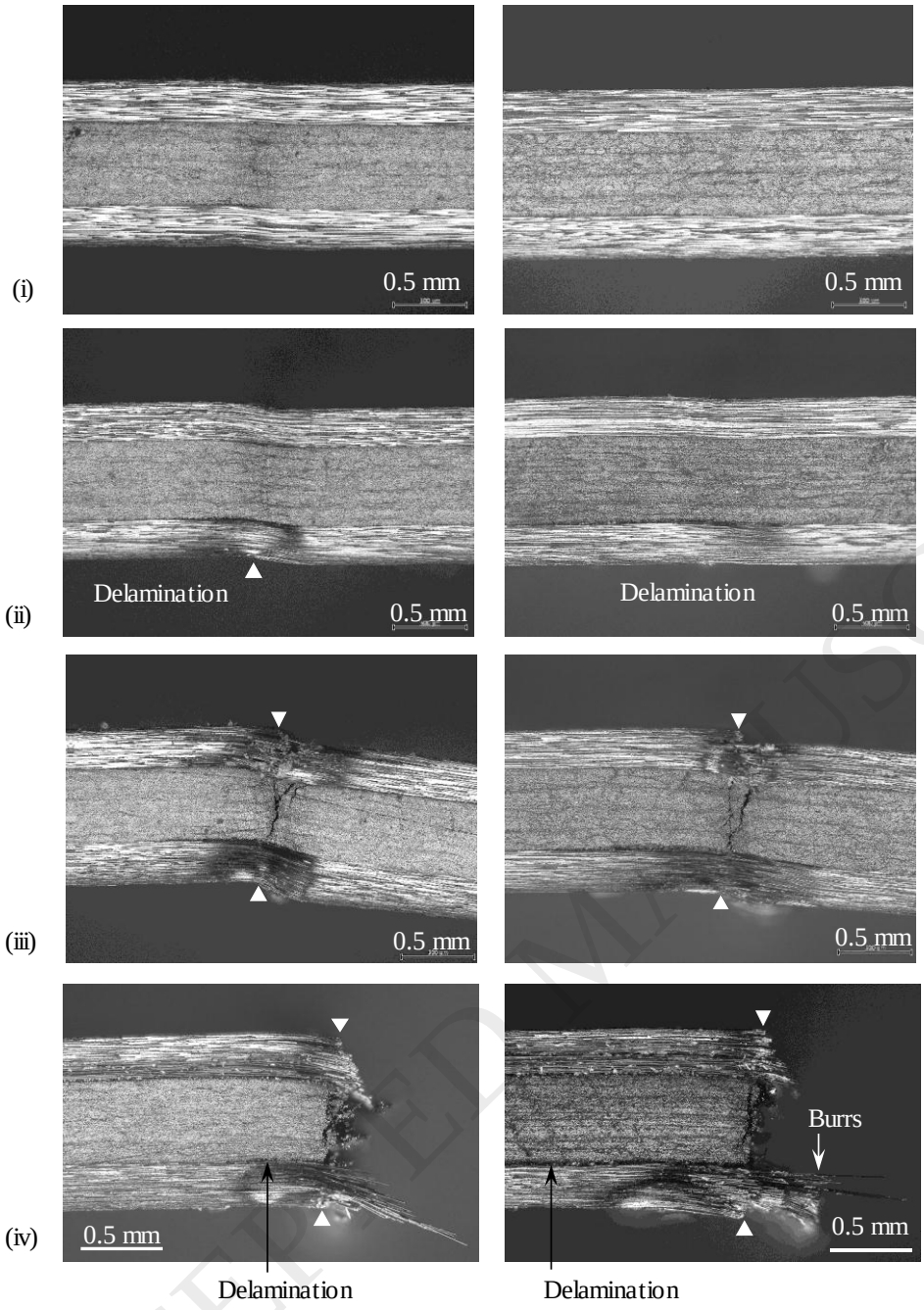

Figure 15 Accumulation of damage in the CP1 specimens tested at high temperatures: (i) after the slight slope change, (ii) before reaching the maximal stress, (iii) after the steep drop in the stress, and (iv) after the complete cut-off. The stress levels (i)-(iv) are indicated in Fig. 14.

Figure 16 shows the edge observations for the CP2 specimens cut at different temperatures.

Similar to the CP1 specimens, the appearance of damage for the samples tested at 70°C was

almost the same as that for the samples tested at room temperature, and delamination was generated at the interface between the second 90° ply and the third 0° ply. The ply interfaces adjacent to the sixth 0° ply were also delaminated at a temperature over T_g, and the micrographs suggest that oblique cracks in the transverse plies induced this delamination. Figure 17 shows the projected delamination area for the CP2 specimens, measured using soft X-ray radiography. The delamination area decreased slightly with an increase in temperature (lower than T_g), but it increased steeply at temperatures above T_g. Double-cantilever beam tests at various temperatures indicated that the interlaminar fracture toughness increased monotonically with an increase in temperature (Nakamura et al., 2015). However, in general, the interlaminar strength degraded significantly at temperatures above T_g. Delamination increased significantly at temperatures above 90°C (approximately T_g) owing to the strength degradation of the ply interfaces.

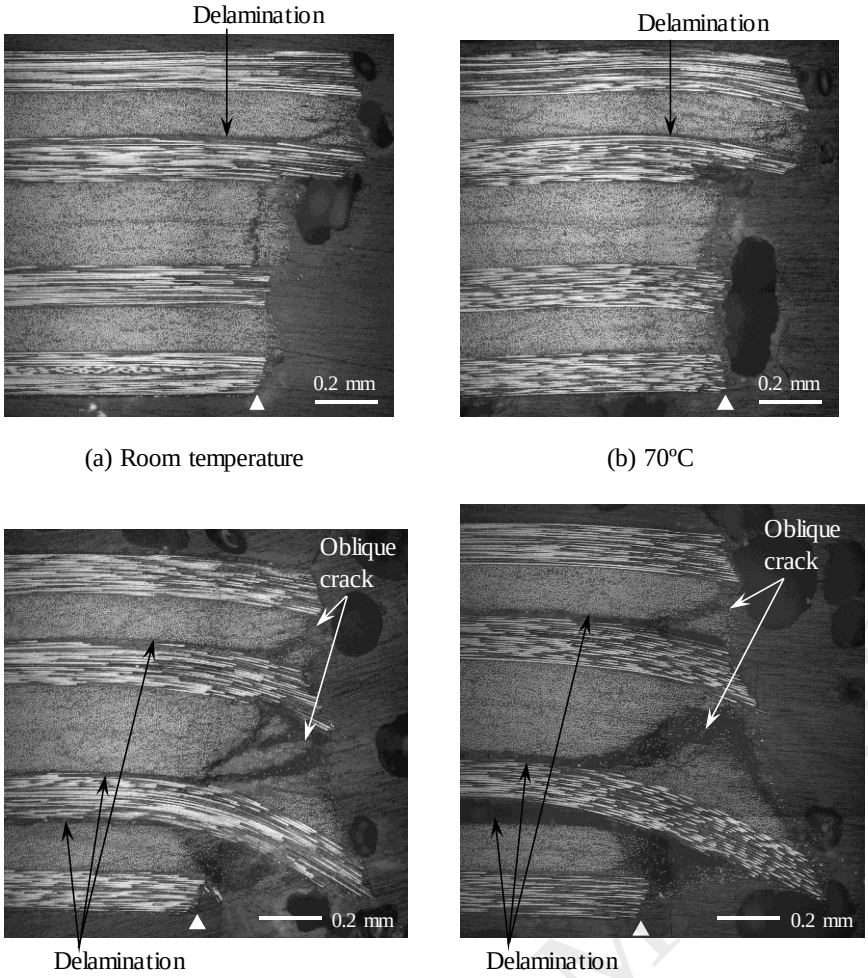

Figure 16 Edge observations for the CP2 specimens after the complete cut-off.

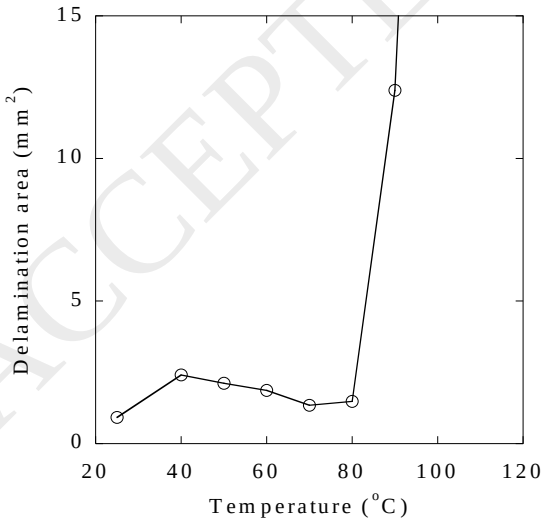

Figure 17 Relationship between the projected delamination area in the CP2 specimens and the temperature.

4. Discussion

In general, machining tools are often degraded by cutting CFRPs. The maximal stress is a major factor that determines the tool's lifetime. Figure 18 shows the relationship between the maximal stress and shearing condition. In our experiments, the maximal shear stress decreased with an increase in clearance and temperature. Although the cutting quality was high for a small clearance condition, a clearance that is too small will reduce the tool's lifetime because of the elevated stress.

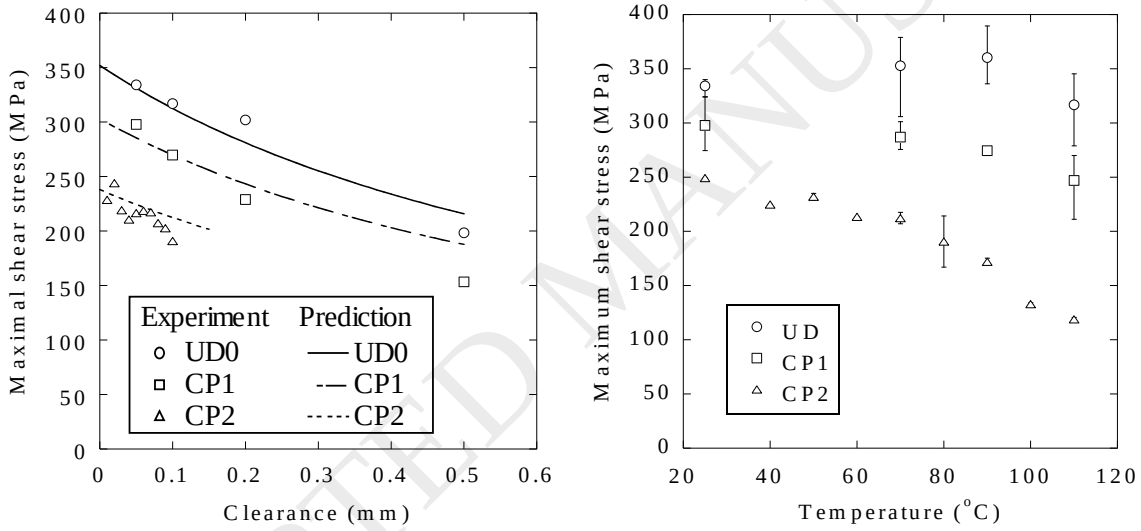

(a) Clearance (room temperature) (b) Temperature (0.05 mm clearance)

Figure 18 Change in the maximal shear stress with the test conditions, where the bars represent the maximal and minimal values for a given condition.

This section presents a mathematical model to predict the maximal shear stress. In our study, shear and bending deformation were observed during the shear cutting process. Onset of fiber breaks can then be predicted using the following empirical failure criterion:

$$\left(\frac{\tau}{\tau_{max}}\right)^n + \left(\frac{\sigma}{F_L}\right)^n = 1 \quad (1)$$

where τ is the nominal shear stress; σ is the maximal bending stress at the surface and is a function of the beam span (i.e., clearance c); τ_{max} is the maximal shear stress under the zero-clearance condition, which depends on the stacking sequence and temperature; F_L is the strength of the 0° ply in the fiber direction; and n is a parameter within a range of 1 to 2. For a laminate with 0° plies on its surfaces, the maximal bending stress at the surface is calculated based on the classical lamination theory as follows:

$$\sigma = Q_{11}\frac{t}{2}\kappa = \frac{Q_{11}t^2c}{2D_{11}}\tau \tag{2}$$

where t is the thickness; Q_{11} is the stiffness in the fiber direction of a unidirectional lamina; D_{11} is the bending stiffness of the tested laminate; and κ (= $\tau tc/D_{11}$) is the curvature generated by the maximal loading, where τtc is the bending moment per unit width. The nominal shear stress is obtained from (1) and (2) as a function of the clearance:

$$\tau = \left\{\left(\frac{1}{\tau_{max}}\right)^n + \left(\frac{Q_{11}t^2c}{2D_{11}F_L}\right)^n\right\}^{-1/n} \tag{3}$$

The prediction by (3) is plotted in Fig. 18a, where the material properties are listed in Table 1a. Note that τ_{max} obtained by linear regression of the experimental data (Table 1b) was used in this calculation. The predictions with n = 1 agreed with the experimental results and confirmed the semi-empirical model.

Table 1 Material properties used in the model.

(a) Mechanical properties	
Longitudinal Young's modulus (GPa)	125
Transverse Young's modulus (GPa)	9.55
In-plane Poisson's ratio	0.25

(b) The maximal shear stress τ_{max} (MPa)	
UD0, RT	352
CP1, RT	303

Longitudinal strength (MPa)	1521 (*1)	CP2, RT	238

(*1) Ueda et al., 2012

The maximal shear stress under the zero-clearance condition, τ_{max}, is then discussed based on the contact theory, and the effect of the stacking sequence on the contact state is estimated. The shear stress distribution obtained by the two-dimensional finite-element analysis of shearing with zero clearance nearly coincided with the analytical solution for a semi-infinite plate subjected to concentrated load. This means that τ_{max} is governed by the contact stress. In the actual shearing process, the tip of the die will make contact with the plate with the finite width. When the contact load distribution is considered to be elliptical, the analytical solution of the shear stress is given as follows (Smith and Liu, 1953):

$$\tau_{xy} = \frac{q_0}{\pi} y^2 G \tag{4}$$

$$G = \frac{\pi}{K_1} \frac{1-\sqrt{K_2/K_1}}{\sqrt{K_2/K_1}\sqrt{2\sqrt{K_2/K_1}+\left(K_1+K_2-4b^2\right)/K_1}} \tag{5}$$

$$K_1 = (b-x)^2 + y^2,\ K_2 = (b+x)^2 + y^2 \tag{6}$$

where q_0 is the maximum of the distributed load and b is half of the contact width. τ_{max} is equivalent to the external load when the maximal shear stress in the stress field reaches 350 MPa (Yashiro and Ogi, DOI: 10.1177/0021998318801454). One half of the contact width, b, can be determined by additional tests and observations. To obtain the values of τ_{max} as listed in Table 1b, b is 0.18, 0.15, and 0.12 mm for UD0, CP1, and CP2, respectively. This difference is interpreted qualitatively by the bending stiffness of the laminates. The CP2 lamination has the smallest bending stiffness among the three laminations and experiences the greatest

deflection, which results in a small contact width near the tip of the die.

The decreasing trend in τ_{max} with increasing temperature is shown in Fig. 18b. However, the reduction is small because the strength of reinforcing fibers as tested with the temperature range in this study hardly changed. By contrast, as Fig. 17 shows, the delamination area increases steeply beyond T_g because mechanical properties of epoxy rapidly change near T_g typically as shown in Fig. 13a. Thus, the glass transition temperature is the threshold that determines the cutting quality (i.e., the appearance of the cut surface and any residual damage).

In terms of material integrity, CFRP laminates should be cut under a small clearance condition at a high temperature that is slightly lower than T_g to minimize the damage. Based on the systematic shearing experiments for the CFRP laminates used in this study, the clearance should be less than 0.1 mm, and the appropriate temperature is 70−80°C. However, in terms of wear of the die, a large clearance increases its lifetime. Thus, these two issues are in trade-off relationship, and an allowable clearance condition needs to be identified using the mathematical model for predicting the nominal shear stress.

5. Concluding remarks

A feasibility study of out-of-shearing for composite laminate plates was conducted. To minimize the damage incurred by out-of-plane shear cutting, this study was done to

systematically investigate the influence of cutting speed, clearance, and temperature on the accumulation of damage in CFRP laminates. The cutting speed had a negligible effect on the shear-cutting process within the tested range of speeds, up to 1000 mm/min. The clearance was important for reducing the damage. In the simple cross-ply laminate, delamination and transverse cracks were generated by the out-of-plane shear loading. A larger clearance reduced the shear stress in the shearing zone but induced greater damage in all of the plies and ply-interfaces, owing to an increased local bending deformation. A small clearance prevented not only delamination but also shear drops of the cut surface. The clearance had significant influence on the maximal shear stress that governs the tool's lifetime. A mathematical model is presented to estimate the maximal stress as a function of the clearance. The effect of temperature was clearly observed in the transverse plies and ply interfaces. Although the interlaminar fracture toughness increased monotonically with an increase in temperature, the strength of the polymer matrix dropped rapidly near T_g, and large delamination appeared at temperatures above T_g. Therefore, a temperature slightly lower than T_g could be the optimal condition for avoiding excessive damage.

References

Alberdi A, Suárez A, Artaza T, Escobar-Palafox GA, Ridgway K. Composite cutting with abrasive water jet. Procedia Engineering 2013; 63:421-429.

Che D, Saxena I, Han P, Guo P, Ehmann KF. Machining of carbon fiber reinforced plastics/polymers: a literature review. J Manuf Sci Eng 2014; 136:034001.

Davim JP, Reis P. Damage and dimensional precision on milling carbon fiber-reinforced plastics using design experiments. J Mater Proc Technol 2005; 160:160-167.

Dubey AK, Yadava V. Laser beam machining—A review. Int J Mach Tools Manuf 2008; 48:609-628.

Fürst A, Mahrle A, Hipp D, Klotzbach A, Hauptmann J, Wetzig A, Beyer E. Dual wavelength laser beam cutting of high- performance composite materials. Adv Eng Mater 2017; 19: 1600356.

Gordon S, Hillery MT. A review of the cutting of composite material. Proc Inst Mech Eng Part L 2003; 217:35-45.

Haddad M, Zitoune R, Bougherara H, Eyma F, Castanié B. Study of trimming damages of CFRP structures in function of the machining processes and their impact on the mechanical behavior. Compos Part B 2014; 57:136-143.

Hejjaji A, Singh D, Kubher S, Kalyanasundaram D, Gururaja S. Machining damage in FRPs: Laser versus conventional drilling. Compos Part A 2016; 82:42-52.

Herzog D, Jaeschke P, Meier O, Haferkamp H. Investigations on the thermal effect caused by laser cutting with respect to static strength of CFRP. Int J Mach Tools Manuf 2008; 48:1464-1473.

Hintze W, Hartmann D, Schütte C. Occurrence and propagation of delamination during the machining of carbon fibre reinforced plastics (CFRPs) – An experimental study. Compos Sci Technol 2011; 71:1719-1726.

Kalla DK, Zhang B, Asmatulu R, Dhanasekaran PS. Current research trends in abrasive waterjet machining of fiber reinforced composites. Mater Sci Forum 2012; 713:37-42.

Leone C, Genna S. Heat affected zone extension in pulsed Nd:YAG laser cutting of CFRP. Compos Part B 2018; 140:174-182.

Li M, Li S, Yang X, Zhang Y, Liang Z. Study on fibre laser machining quality of plain woven CFRP laminates. Appl Phys A 2018; 124:270.

Li M, Huang M, Yang X, Li S, Wei K. Experimental study on hole quality and its impact on tensile behavior following pure and abrasive waterjet cutting of plain woven CFRP laminates. Int J Adv Manuf Technol 2018; 99:2481-2490.

Li ZL, Zheng HY, Lim GC, Chu PL, Li L. Study on UV laser machining quality of carbon fibre reinforced composites. Compos Part A 2010; 41:1403-1408.

MM IW, Azumi AI, Lee CC, Mansor AF. Kerf taper and delamination damage minimization of FRP hybrid composites under abrasive water-jet machining. Int J Adv Manuf Technol

2018; 94:1727-1744.

Nakamura N, Ogi K, Ota A, Nakata S, Suma K. Shear cutting behaviors in thermosetting and thermoplatic CFRP laminates. Key Eng Mater 2015; 656-657: 347-352.

Persson E, Eriksson I, Zackrisson L. Effects of hole machining defects on strength and fatigue life of composite laminates. Compos Part A 1997; 28:141-151.

Saleem M, Toubal L, Zitoune R, Bougherara H. Investigating the effect of machining processes on the mechanical behavior of composite plates with circular holes. Compos Part A 2013; 55:169-177.

Schwartzentruber J, Papini M, Spelt JK. Characterizing and modelling delamination of carbon-fiber epoxy laminates during abrasive waterjet cutting. Compos Part A 2018; 112:299-314.

Shanmugam DK, Chen FL, Siores E, Brandt M. Comparative study of jetting machining technologies over laser machining technology for cutting composite materials. Compos Struct 2002; 57:289-296.

Shanmugam DK, Nguyen T, Wang J. A study of delamination on graphite/epoxy composites in abrasive waterjet machining. Compos Part A 2008; 39:923-929.

Sheikh-Ahmad J, Urban N, Cheraghi H. Machining damage in edge trimming of CFRP. Mater Manuf Process 2012; 27:802-808.

Smith JO, Liu CK. Stresses due to tangential and normal loads on an elastic solid with

application to some contact stress problems. J Appl Mech 1953; 20:157-166.

Soussia AB, Mkaddem A, Mansori ME. Rigorous treatment of dry cutting of FRP - Interface consumption concept: A review. Int J Mech Sci 2014; 83:1-29.

Tatsuno D, Yoneyama T, Kawamoto K and Okamoto M. Production system to form, cut, and join by using a press machine for continuous carbon fiber-reinforced thermoplastic sheets. Polym Compos 2018; 39:2571-2586.

Teti R. Machining of composite materials. CIRP Annals 2002; 51:611-634.

Ueda M, Ishii M, Nishimura T. Estimating compressive strength of unidirectional CFRP using apparent shear modulus. J. Japan Soc Compos Mater 2012; 38:15-21. (in Japanese)

Yashiro S, Ono R, Ogi K, Sakaida Y. Prediction of shear-cutting process of CFRP cross-ply laminates using smoothed particle hydrodynamics. In: Proc. 16th US-Japan Conference on Composite Materials. San Diego, USA, 8-10 September 2014. Paper No. 747.

Yashiro S, Ogi K. Experimental study on shear-dominant fiber failure in CFRP laminates by out-of-plane shear loading. J Compos Mater; in press, DOI: 10.1177/0021998318801454.

Yashiro T, Ogawa T, Sasahara H. Temperature measurement of cutting tool and machined surface layer in milling of CFRP. Int J Mach Tools Manuf 2013; 70:63-69.

Wang J. Abrasive waterjet machining of polymer matrix composites - cutting performance, erosive process and predictive models. Int J Adv Manuf Technol 1999; 15:757-768.

Watzke J, Schomäcker M, Brosius A. Cryogenic shear cutting of fiber reinforced plastics (FRP). Procedia CIRP 2014; 18:80-83.

Figure captions

Fig. 1 Morphology of a composite laminate. The CP1 lamination is depicted as an example.

Fig. 2 Schematic of the out-of-plane shearing jig.

Fig. 3 Shear stress-displacement curves for the UD0 specimens, for different indentation speeds.

Fig. 4 Inclination of the cut surface against the bottom plane. Error bars in panel (b) indicate the standard deviation.

Fig. 5 Shear stress-displacement curves for the UD0 specimens, for four clearances.

Fig. 6 Edge observations for the UD0 specimen after the onset of fiber breaks. Triangles indicate the tips of the upper and lower dies.

Fig. 7 Shear stress-displacement curves for the UD90 specimens, for four clearances. In the case of 0.1 mm and 0.2 mm clearances, two-peak curves were also obtained for some specimens.

Fig. 8 Edge observations for the UD90 specimens immediately prior to the complete cut-off.

Fig. 9 Shear stress-displacement curves for the CP1 specimens, for four clearances.

Fig. 10 Accumulation of damage in the CP1 specimens tested at room temperature: (i) after slight slope change, (ii) before reaching the maximal stress, (iii) after the steep drop

in the stress, and (iv) after further indentation for complete cut-off. The stress levels (i)-(iv) are indicated in Fig. 9.

Fig. 11 Cut quality of the CP1 specimens, vs. the clearance.

Fig. 12 Results for the UD0 specimens, for four temperatures.

Fig. 13 Results for the UD90 specimens, for four temperatures.

Fig. 14 Shear-stress displacement curves for the CP1 specimens, for four temperatures.

Fig. 15 Accumulation of damage in the CP1 specimens tested at high temperatures: (i) after the slight slope change, (ii) before reaching the maximal stress, (iii) after the steep drop in the stress, and (iv) after the complete cut-off. The stress levels (i)-(iv) are indicated in Fig. 14.

Fig. 16 Edge observations for the CP2 specimens after the complete cut-off.

Fig. 17 Relationship between the projected delamination area in the CP2 specimens and the temperature.

Fig. 18 Change in the maximal shear stress with the test conditions, where the bars represent the maximal and minimal values for a given condition.